Higgs boson production at large transverse momentum within the SMEFT: analytical results

Originally published in:
The European Physical Journal C 78, https://doi.org/10.1140/epjc/s10052-018-6261-7

Funding acknowledgement:
316704 - The Higgs quest - exploring electroweak symmetry breaking at the LHC (EC)

Eur. Phys. J. C (2018) 78:808
https://doi.org/10.1140/epjc/s10052-018-6261-7

THE EUROPEAN PHYSICAL JOURNAL C

Regular Article - Theoretical Physics

Higgs boson production at large transverse momentum within the SMEFT: analytical results

Massimiliano Grazzini[1,a], **Agnieszka Ilnicka**[1,2,3], **Michael Spira**[3]

[1] Physik-Institut, Universität Zürich, 8057 Zurich, Switzerland
[2] Physics Department, ETH Zürich, 8093 Zurich, Switzerland
[3] Paul Scherrer Institut PSI, 5232 Villigen, Switzerland

Received: 4 July 2018 / Accepted: 19 September 2018 / Published online: 4 October 2018

Abstract We consider Higgs boson production through gluon fusion at large transverse momentum in hadronic collisions. We present the analytic expressions of the relevant one-loop QCD amplitudes including the effects of the complete set of dimension-six operators. The latter correspond to modifications of the top and bottom Yukawa couplings, to an effective point-like Higgs coupling to gluons and to the chromomagnetic operator of the top quark. The quantitative impact of the chromomagnetic operator is also studied. Our results confirm previous findings that the effect of the chromomagnetic operator at high p_T can be large and should not be neglected.

1 Introduction

After the discovery of the scalar resonance of mass 125 GeV [1,2] the measurement of its properties is one of the main activities of the LHC program. The Run I measurements [3] showed that the new resonance is compatible with the Standard Model Higgs boson. There is, however, still the possibility that more precise measurements will uncover small deviations from the Standard Model (SM) predictions. These might be the long lasting legacy of the LHC, which will encompass the searches for New Physics. The need of a consistent framework to capture small deviations from the SM is reflected in the wide discussions in Refs. [4–6]. The Standard Model Effective Field Theory (SMEFT) is a promising and theory motivated approach, in which the deviations from the SM are parametrised with higher-dimension operators, in the first approximation dimension six [7,8].

Next to the inclusive quantities, differential Higgs observables were measured in Run I [9–15] and with a partial data set of Run II [16–18], although still with relatively large uncertainties. With the increasing amount of collected data, the statistical accuracy will improve, thereby allowing us to put stringent constraints on the SMEFT parameters. One of the observables which is able to shed light on the structure of the Higgs sector is the transverse momentum spectrum (p_T) of the Higgs particle. For example, a measurement of the p_T spectrum could give insight on the nature of the Higgs boson coupling to gluons (see e.g. Refs. [19,20]).

Recent years have seen considerable progress in the theoretical control of the p_T spectrum in the SM [21–27]. In particular, the NLO QCD corrections are now available including the exact dependence on the top-quark mass [28].

Dedicated calculations and tools are needed to enable the experimental analyses to set bounds on the SMEFT operators. Approximate results for the total gluon fusion Higgs production cross section including modified top and bottom Yukawa couplings and an additional direct Hgg interaction have been obtained at NNLO in QCD perturbation theory in Ref. [29] and at N^{3}LO in Refs. [30,31]. As far as gluon fusion is concerned, the inclusion of dimension-six and dimension-eight operators in the Higgs p_T-spectrum also has been considered in Refs. [32–34] and [35,36], respectively. Strategies for extracting information on the Higgs-gluon couplings from the measurements were studied in Ref. [34], and the study the low-p_T range therein was made possible by using Monte Carlo Parton Shower. Also in Ref. [20] the prospects of the determination of the Wilson coefficients in the high-luminosity LHC and future colliders were considered. The mentioned studies usually omitted the effects of the chromomagnetic operator, but a dedicated work analysed its effect on the LO Higgs production [37]. This was followed by a LO study [38] on the interplay of the SMEFT operators entering top-induced Higgs production channels, with the chromomagnetic operator treated in the heavy-top limit (HTL). Recently, the program of the SMEFT at NLO QCD was started by the MADGRAPH5_AMC@NLO group

[a] e-mail: grazzini@physik.uzh.ch

[39] and led to the calculation of $t\bar{t}H$, tH [40] and recently also of Higgs production through gluon fusion [41].

In this work we recall the results for the LO Higgs production via gluon fusion and we extend our study [42] of the Higgs p_T spectrum to include the effects of the chromomagnetic operator. More precisely, we present the analytic expressions of the relevant one-loop QCD amplitudes including the effects of the complete set of dimension-six operators and we shortly illustrate the impact of the chromomagnetic operator on the high-p_T tail of the spectrum. Note that, due to the automated character of the calculations in the MadGraph5_aMC@NLO framework [40,41], they can be considered complementary to the analytic calculations presented here.

The paper is organised as follows. In Sect. 1 we review the LO results and set up our notation. In Sect. 2 we present the analytical results for the SMEFT one-loop QCD amplitudes in all partonic channels, and we briefly discuss the impact of the chromomagnetic operator at high p_T. In Sect. 4 we draw our conclusions.

2 Framework and LO results

We consider the effective Lagrangian

$$\mathcal{L} = \mathcal{L}_{SM} + \sum_i \frac{c_i}{\Lambda^2}\mathcal{O}_i, \tag{1}$$

where the SM is supplemented by the inclusion of a set of dimension-six operators describing new physics effects at a scale Λ well above the EW scale. We focus on the following three operators

$$\mathcal{O}_1 = |H|^2 \bar{q}_L H^c t_R + h.c. \quad \mathcal{O}_2 = |H|^2 G^a_{\mu\nu} G^{a,\mu\nu}$$
$$\mathcal{O}_3 = \bar{Q}_L H \sigma^{\mu\nu} T^a t_R G^a_{\mu\nu} + h.c. \tag{2}$$

These operators, in the case of single Higgs production, may be rewritten as:

$$\frac{c_1}{\Lambda^2}\mathcal{O}_1 \to c_1 \frac{m_t}{v} h\bar{t}t\,, \tag{3}$$
$$\frac{c_2}{\Lambda^2}\mathcal{O}_2 \to c_2 \frac{\alpha_S}{\pi v} h G^a_{\mu\nu} G^{a,\mu\nu}\,, \tag{4}$$
$$\frac{c_3}{\Lambda^2}\mathcal{O}_3 \to c_3 \frac{g_S m_t}{2v^3}(v+h) G^a_{\mu\nu}(\bar{t}_L \sigma^{\mu\nu} T^a t_R + h.c), \tag{5}$$

where α_S is the QCD coupling ($\alpha_S = g_S^2/(4\pi)$), m_t is the (pole) mass of the top quark, v is the expectation value of the Higgs field, $v = (\sqrt{2}G_F)^{-1/2} \sim 246$ GeV and $\sigma^{\mu\nu} = \frac{i}{2}\left[\gamma^\mu, \gamma^\nu\right]$. The operator $\mathcal{O}_1$ is the Yukawa operator, and describes modifications of the $t\bar{t}H$ coupling. The operator $\mathcal{O}_2$ provides a contact interaction of the Higgs boson and gluons with the same structure as in the heavy-top limit of the SM. The operator $\mathcal{O}_3$ is the chromomagnetic dipole moment operator, which modifies the interactions between gluons and the top quark. In our convention, based on the SILH basis [43,44], we express the Wilson coefficients as factors in the canonically normalized Lagrangian.

To set up our convention we reproduce the results for the LO inclusive cross section for $gg \to H$ as exemplified in Refs. [42,45,46]. After renormalizing the point-like Higgs-gluon coupling c_2 in the $\overline{\text{MS}}$ scheme the LO matrix element can be decomposed as

$$\mathcal{T}_{gg\to H}(p_1, p_2) = i\frac{\alpha_S}{3\pi v}\epsilon_\mu(p_1)\epsilon_\nu(p_2) \times \left[p_1^\nu p_2^\mu - (p_1 p_2) g^{\mu\nu}\right] F(\tau_H), \tag{6}$$

where p_1, p_2 are the gluon momenta, $\epsilon(p_1)$, $\epsilon(p_2)$ their polarisations and $\tau_H = 4m_t^2/m_H^2$, m_H being the Higgs boson mass. The form factor $F(\tau)$ is defined as

$$F(\tau) = c_1 F_1(\tau) + c_2(\mu_R) F_2(\tau) + Re(c_3)\frac{m_t^2}{v^2} F_3(\tau), \tag{7}$$

with[1]

$$F_1(\tau) = \frac{3}{2}\tau\left[1 + (1-\tau) f(\tau)\right], \tag{8}$$
$$F_2(\tau) = 12, \tag{9}$$
$$F_3(\tau) = 3\left(\tau f(\tau) + 2g(\tau) - 1 - 2\ln\frac{\mu_R^2}{m_t^2}\right) \tag{10}$$

and the functions f, g are defined in "Appendix". In the HTL the form factors approach the simple expressions

$$F_1(\tau) \to 1\,, \tag{11}$$
$$F_2(\tau) \to 12, \tag{12}$$
$$F_3(\tau) \to 6\left(1 - \ln\frac{\mu_R^2}{m_t^2}\right). \tag{13}$$

3 Higgs plus jet production

Higgs boson production in association with a jet is the LO contribution to Higgs boson production at finite transverse momenta. This process is mediated by gg, gq and $q\bar{q}$ initial states. We start the presentation of our results for the gg channel,

$$g(p_1) + g(p_2) \to g(p_3) + H(q)$$

and the Mandelstam variables are defined as

$$s = 2p_1 \cdot p_2 \qquad t = -2p_1 \cdot p_3$$
$$u = -2p_2 \cdot p_3 \qquad \text{with} \qquad s + t + u = m_H^2\,. \tag{14}$$

[1] Note that we changed our sign convention of c_3 compared to Ref. [42].

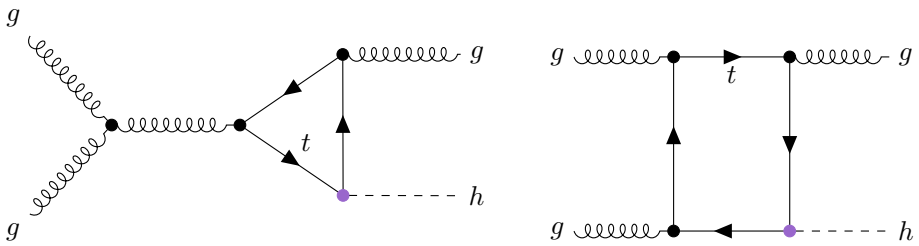

Fig. 1 Generic diagrams originating from the $\mathcal{O}_1$ operator that also provide the SM contribution

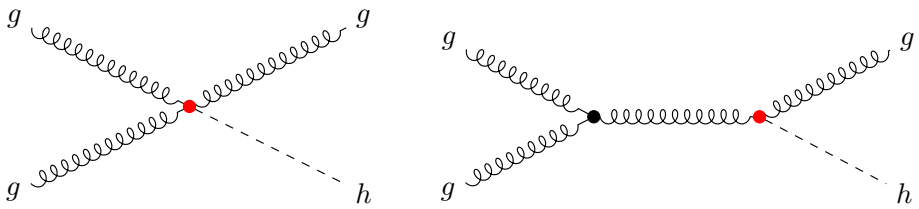

Fig. 2 Generic diagrams originating from the $\mathcal{O}_2$ operator. These correspond also to the effective SM diagrams in the HTL

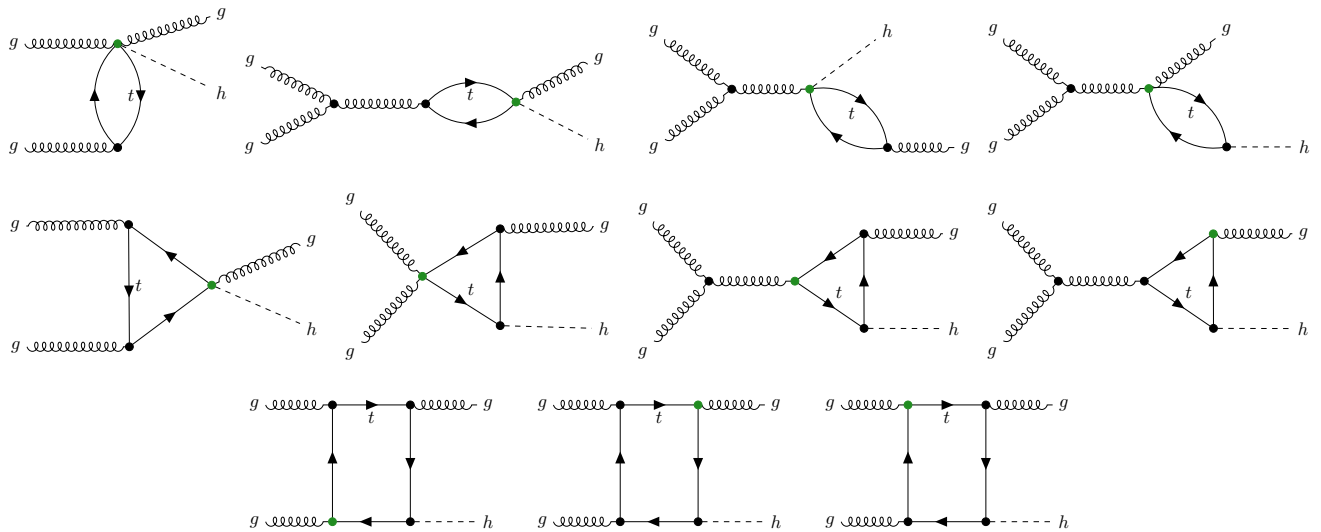

Fig. 3 Generic diagrams induced by the chromomagnetic operator $\mathcal{O}_3$

The contributing generic SM diagrams are shown in Fig. 1.

The contribution from the modified Yukawa coupling can be straightforwardly obtained by rescaling the SM result. The effective Higgs-gluon coupling gives rise to the diagrams in Fig. 2. When considering the insertion of the chromomagnetic operator we obtain 54 additional diagrams (see Fig. 3) out of which just 2 types are topologically equivalent to the SM ones.

The amplitude can be cast into the form

$$\mathcal{T}_{gg\to gH}(p_1, p_2, p_3) = \frac{ig_S^3 m_H^4}{12\pi^2 v} f_{abc} \mathcal{M}^{\mu\nu\rho}_{gg\to gH} \epsilon_\mu(p_1)\epsilon_\nu(p_2)\epsilon^*_\rho(p_3), \tag{15}$$

where $\epsilon(p_i)$ are the gluon polarisation vectors. The amplitude can be decomposed into four independent tensor structures [47]

$$\begin{aligned}\mathcal{M}^{\mu\nu\rho}_{gg\to gH}(p_1, p_2, p_3) &= F_1(p_1, p_2, p_3)\mathcal{Q}_1^{\mu\nu\rho} \\ &+ F_2(p_1, p_2, p_3)\mathcal{Q}_2^{\mu\nu\rho} \\ &+ F_3(p_1, p_2, p_3)\mathcal{Q}_3^{\mu\nu\rho} + F_4(p_1, p_2, p_3)\mathcal{Q}_4^{\mu\nu\rho}\end{aligned} \tag{16}$$

where

$$\begin{aligned}\mathcal{Q}_1^{\mu\nu\rho} &= p_1^\rho p_2^\mu p_3^\nu - p_1^\nu p_2^\rho p_3^\mu \\ &+ g^{\mu\nu}[(p_1\cdot p_3)p_2^\rho - (p_2\cdot p_3)p_1^\rho] \\ &+ g^{\mu\rho}[(p_2\cdot p_3)p_1^\nu - (p_1\cdot p_2)p_3^\nu] \\ &+ g^{\nu\rho}[(p_1\cdot p_2)p_3^\mu - (p_1\cdot p_3)p_2^\mu]\end{aligned}$$

$$\mathcal{Q}_2^{\mu\nu\rho} = [(p_2\cdot p_3)p_1^\rho - (p_1\cdot p_3)p_2^\rho]\frac{p_1^\nu p_2^\mu - (p_1\cdot p_2)g^{\mu\nu}}{(p_1\cdot p_2)}$$

$$\mathcal{Q}_3^{\mu\nu\rho} = [(p_2\cdot p_3)p_1^\nu - (p_1\cdot p_2)p_3^\nu]\frac{p_1^\rho p_3^\mu - (p_1\cdot p_3)g^{\mu\rho}}{(p_1\cdot p_3)}$$
$$\mathcal{Q}_4^{\mu\nu\rho} = [(p_1\cdot p_3)p_2^\mu - (p_1\cdot p_2)p_3^\mu]\frac{p_2^\rho p_3^\nu - (p_2\cdot p_3)g^{\nu\rho}}{(p_2\cdot p_3)}\,. \tag{17}$$

It is useful to note that based on the definitions of the tensor structures the form factors have the following properties due to Bose symmetry,

$$\begin{aligned} F_2(p_1,p_2,p_3) &= F_2(p_2,p_1,p_3) \\ &= -F_3(p_1,p_3,p_2) = F_4(p_3,p_2,p_1) \end{aligned} \tag{18}$$

and F_1 is totally symmetric. When squaring the amplitude, the decomposition in Eq. (16) leads to mixed terms in the form factors F_i. If we rearrange the form factors as

$$\begin{aligned} C_1(s,t,u;m_t) &= \frac{stu}{2}\,[2F_1(p_1,p_2,p_3) + F_2(p_1,p_2,p_3) \\ &\quad - F_3(p_1,p_2,p_3) + F_4(p_1,p_2,p_3)] \\ C_2(s,t,u;m_t) &= \frac{stu}{2}\,F_2(p_1,p_2,p_3) \\ C_3(s,t,u;m_t) &= \frac{stu}{2}\,F_3(p_1,p_2,p_3) \\ C_4(s,t,u;m_t) &= \frac{stu}{2}\,F_4(p_1,p_2,p_3), \end{aligned} \tag{19}$$

where the C_i develop the analogous Bose-symmetry properties as the previous form factors

$$\begin{aligned} C_3(s,t,u;m_t) &= -C_2(t,s,u;m_t) \\ C_4(s,t,u;m_t) &= C_2(u,t,s;m_t) \end{aligned} \tag{20}$$

the amplitude squared can now be expressed as a sum of absolute squares

$$|\mathcal{T}_{gg\to gH}|^2 = \frac{32\alpha_S^3}{3\pi v^2}\frac{m_H^8}{stu}(|C_1|^2 + |C_2|^2 + |C_3|^2 + |C_4|^2). \tag{21}$$

Here we present the results for $C_1(s,t,u;m_t)$ and $C_2(s,t,u;m_t)$ (C_3 and C_4 can be obtained from C_2 following Eq. (20)) in terms of the scalar integrals:

$$C_i^{(\alpha)} = \frac{1}{32}\tau_H^2\sum_{j=1}^{12} P_{i,j}^{(\alpha)}\,T_j, \tag{22}$$

where the α index runs over the operators $\mathcal{O}_\alpha$ in Eq. (2) and

$$T_1 = 1 \qquad T_2 = 2\,[1 - g\,(\tau_s)] \tag{23}$$

$$T_3 = 2\,[1 - g\,(\tau_t)] \qquad T_4 = 2\,[1 - g\,(\tau_u)] \tag{24}$$
$$T_5 = 2[1 - g(\tau_H)] \qquad T_6 = 2\,f(\tau_s) \tag{25}$$
$$T_7 = 2\,f(\tau_t) \qquad T_8 = 2\,f(\tau_u) \tag{26}$$
$$T_9 = 2\,f(\tau_H) \qquad T_{10} = J(\tilde{s},\tilde{t},\tilde{u}) \tag{27}$$
$$T_{11} = J(\tilde{s},\tilde{u},\tilde{t}) \qquad T_{12} = J(\tilde{u},\tilde{s},\tilde{t})\,. \tag{28}$$

In order to present our results in a compact form we have defined dimensionless quantities $\tilde{x} = x/m_t^2$ and $\tau_x = 4/\tilde{x}$ for $x = s,t,u$ and $\rho = m_H^2/m_t^2$. The scalar functions $f(x)$, $g(x)$ and $J(x,y,z)$ are given in "Appendix". The $P_{i,j}^{(1)}$ coefficients, corresponding to the SM contribution, read

$$\begin{aligned} P_{1,1}^{(1)} &= 12\rho & P_{1,2}^{(1)} &= 0 \\ P_{1,3}^{(1)} &= 0 & P_{1,4}^{(1)} &= 0 \\ P_{1,5}^{(1)} &= 0 & P_{1,6}^{(1)} &= 3(4-\rho) \\ P_{1,7}^{(1)} &= 3(4-\rho) & P_{1,8}^{(1)} &= 3(4-\rho) \\ P_{1,9}^{(1)} &= -9(4-\rho) & P_{1,10}^{(1)} &= \tfrac{3}{2}\tilde{s}\tilde{u}(4-\rho) \\ P_{1,11}^{(1)} &= \tfrac{3}{2}\tilde{s}\tilde{t}(4-\rho) & P_{1,12}^{(1)} &= \tfrac{3}{2}\tilde{t}\tilde{u}(4-\rho) \end{aligned} \tag{29}$$

$$P_{2,1}^{(1)} = -12\tilde{s}\frac{\tilde{u}\tilde{t} - \tilde{s}^2}{(\tilde{s}+\tilde{u})(\tilde{s}+\tilde{t})}$$
$$P_{2,2}^{(1)} = 0$$
$$P_{2,3}^{(1)} = \frac{12\tilde{t}\tilde{u}\,(\tilde{u}+2\tilde{s})}{(\tilde{s}+\tilde{u})^2}$$
$$P_{2,4}^{(1)} = \frac{12\tilde{t}\tilde{u}\,(\tilde{t}+2\tilde{s})}{(\tilde{s}+\tilde{t})^2}$$
$$P_{2,5}^{(1)} = -\frac{12\tilde{t}\tilde{u}}{(\tilde{s}+\tilde{t})^2(\tilde{s}+\tilde{u})^2}\left[(3\tilde{s}^2+\tilde{t}\tilde{u}+2\rho\tilde{s})(\rho-\tilde{s}) + 4\tilde{s}^3\right]$$
$$P_{2,6}^{(1)} = -3(\tilde{s}-4)$$
$$P_{2,7}^{(1)} = -\frac{3\left(4\tilde{t}\tilde{u}(\tilde{s}+\tilde{u})^2 + \tilde{s}(4-\tilde{s})(\tilde{u}^2-\tilde{s}^2) + 8\tilde{s}^2\tilde{u}\right)}{\tilde{s}(\tilde{s}+\tilde{u})^2}$$
$$P_{2,8}^{(1)} = -\frac{3\left(4\tilde{t}\tilde{u}(\tilde{s}+\tilde{t})^2 + \tilde{s}(4-\tilde{s})(\tilde{t}^2-\tilde{s}^2) + 8\tilde{s}^2\tilde{t}\right)}{\tilde{s}(\tilde{s}+\tilde{t})^2}$$
$$\begin{aligned} P_{2,9}^{(1)} &= \frac{3}{\tilde{s}(\tilde{s}+\tilde{t})^2(\tilde{s}+\tilde{u})^2}\left\{4\tilde{u}(\tilde{s}+\tilde{t})^2[2\tilde{s}^2+\tilde{t}(\tilde{s}+\tilde{u})^2]\right. \\ &\quad +8\tilde{s}^4\tilde{t} + 4\tilde{s}^2\tilde{t}\tilde{u}(\tilde{s}^2+2\tilde{u}) \\ &\quad \left.+\tilde{s}(\tilde{s}-4)[\tilde{s}^2[(\tilde{s}+\tilde{t})^2+(\tilde{s}+\tilde{u})^2] + \tilde{s}^3(2\rho-\tilde{s}) - \tilde{t}^2\tilde{u}^2]\right\} \end{aligned}$$
$$P_{2,10}^{(1)} = \frac{3\tilde{s}\tilde{u}(4-\tilde{s})}{2}$$
$$P_{2,11}^{(1)} = \frac{3\tilde{s}\tilde{t}(4-\tilde{s})}{2}$$
$$P_{2,12}^{(1)} = -\frac{3\tilde{t}\tilde{u}\left(4\tilde{t}\tilde{u} - \tilde{s}^2 + 12\tilde{s}\right)}{2\tilde{s}}\,. \tag{30}$$

This result agrees with the one presented in Refs. [47–49].

The coefficients for the contribution arising from the chromomagnetic operator read

$$
\begin{aligned}
&P^{(3)}_{1,1} = 6\rho^2\left(1-2\log\tfrac{\mu_R^2}{m_t^2}\right) && P^{(3)}_{1,2} = -6\tilde{t}\tilde{u}\\
&P^{(3)}_{1,3} = -6\tilde{s}\tilde{u} && P^{(3)}_{1,4} = -6\tilde{s}\tilde{t}\\
&P^{(3)}_{1,5} = -6\rho^2 && P^{(3)}_{1,6} = -3\left(2\rho-\tilde{t}\tilde{u}\right)\\
&P^{(3)}_{1,7} = -3\left(2\rho-\tilde{s}\tilde{u}\right) && P^{(3)}_{1,8} = -3\left(2\rho-\tilde{s}\tilde{t}\right)\\
&P^{(3)}_{1,9} = 18\rho && P^{(3)}_{1,10} = -3\tilde{s}\tilde{u}(\rho+\tilde{t})\\
&P^{(3)}_{1,11} = -3\tilde{s}\tilde{t}(\rho+\tilde{u}) && P^{(3)}_{1,12} = -3\tilde{t}\tilde{u}(\rho+\tilde{s})
\end{aligned}
\tag{31}
$$

$$
\begin{aligned}
P^{(3)}_{2,1} &= \frac{6\rho\tilde{s}\left(\tilde{s}^2-\tilde{t}\tilde{u}\right)}{(\tilde{s}+\tilde{t})(\tilde{s}+\tilde{u})} - 12\tilde{s}^2\log\frac{\mu_R^2}{m_t^2}\\
P^{(3)}_{2,2} &= 0\\
P^{(3)}_{2,3} &= \frac{6\tilde{t}\tilde{u}\left(\rho^2-\tilde{t}(\tilde{t}+\tilde{u})\right)}{(\tilde{s}+\tilde{u})^2}\\
P^{(3)}_{2,4} &= \frac{6\tilde{t}\tilde{u}\left(\rho^2-\tilde{u}(\tilde{t}+\tilde{u})\right)}{(\tilde{s}+\tilde{t})^2}\\
P^{(3)}_{2,5} &= -\frac{6\rho}{(\tilde{s}+\tilde{t})^2(\tilde{s}+\tilde{u})^2}(\rho\tilde{s}^2(\tilde{s}^2+4\tilde{t}\tilde{u})\\
&\quad + 2\tilde{s}\tilde{t}\tilde{u}(\rho-\tilde{s})^2 - \tilde{t}^2\tilde{u}^2(2\tilde{s}-\rho))\\
P^{(3)}_{2,6} &= -6(2\tilde{s}-\rho)\\
P^{(3)}_{2,7} &= -\frac{3\left\{(\tilde{s}+\tilde{u})^2\left[2\rho(\tilde{s}+\tilde{t}\tilde{u})-\tilde{s}\tilde{t}\tilde{u}\right]-4\tilde{s}^2[\tilde{s}(\rho-\tilde{s})+\tilde{u}^2]\right\}}{\tilde{s}(\tilde{s}+\tilde{u})^2}\\
P^{(3)}_{2,8} &= -\frac{3\left\{(\tilde{s}+\tilde{t})^2\left[2\rho(\tilde{s}+\tilde{t}\tilde{u})-\tilde{s}\tilde{t}\tilde{u}\right]-4\tilde{s}^2[\tilde{s}(\rho-\tilde{s})+\tilde{t}^2]\right\}}{\tilde{s}(\tilde{s}+\tilde{t})^2}\\
P^{(3)}_{2,9} &= \frac{3}{\tilde{s}(\tilde{s}+\tilde{t})^2(\tilde{s}+\tilde{u})^2}\\
&\quad\times\left\{2\tilde{s}\left[3\rho\tilde{s}^4+\tilde{s}(2\tilde{t}\tilde{u}-\rho\tilde{s})(\rho-\tilde{s})^2+2\tilde{s}^2\tilde{t}\tilde{u}(\tilde{s}+4\rho)\right.\right.\\
&\quad\left.\left.+\tilde{t}^2\tilde{u}^2(\rho-2\tilde{s})\right]+\tilde{t}\tilde{u}(\tilde{s}+\tilde{t})^2(\tilde{s}+\tilde{u})^2(2\rho-\tilde{s})\right\}\\
P^{(3)}_{2,10} &= -3\tilde{s}\tilde{u}(\tilde{s}-\tilde{u})\\
P^{(3)}_{2,11} &= -3\tilde{s}\tilde{t}(\tilde{s}-\tilde{t})\\
P^{(3)}_{2,12} &= -\frac{3\tilde{t}\tilde{u}\left[2(\rho-\tilde{s})(3\tilde{s}+\tilde{t}\tilde{u})+\tilde{s}\tilde{t}\tilde{u}\right]}{2\tilde{s}}\,.
\end{aligned}
\tag{32}
$$

The log $\frac{\mu_R^2}{m_t^2}$ terms arise from the absorption of the $1/\epsilon$ divergence in the renormalisation of the c_g coupling. For the effective Higgs coupling to gluons we directly present the expressions of the C_1 and C_2 form factors, which read

$$
\begin{aligned}
C_1^{(2)}(s,t,u;m_t) &= 12\\
C_2^{(2)}(s,t,u;m_t) &= \frac{12s^2}{m_H^4},
\end{aligned}
\tag{33}
$$

which correspond also to the HTL of the SM result multiplied by a factor of 12. For completeness we report the HTL also for the contribution of the chromomagnetic operator

$$
C_i^{(3)} \to \frac{1}{2}\left(1-\ln\frac{\mu_R^2}{m_t^2}\right)C_i^{(2)} \quad i=1,2.
$$

The final results for the form factors C_i read

$$
\begin{aligned}
C_i(s,t,u;m_t) &= c_1 C_i^{(1)}(s,t,u;m_t)\\
&\quad + c_2(\mu_R)C_i^{(2)}(s,t,u;m_t) + Re(c_3)\frac{m_t^2}{v^2}C_i^{(3)}(s,t,u;m_t).
\end{aligned}
\tag{34}
$$

We now move to the $q\bar{q}$ channel:

$$
q(p_1)+\bar{q}(p_2) \to g(p_3)+H(q)\,.
$$

The contributing generic Feynman diagrams are depicted in Fig. 4.

The corresponding amplitude can be decomposed as

$$
\begin{aligned}
\mathcal{M}_{q\bar{q}\to gH}(p_1,p_2,p_3) &= \frac{ig_S^3}{16\pi^2 vs}\bar{v}(p_2)\gamma^\mu T^a u(p_1)\\
&\quad\times\left[g_{\mu\nu}(p_1+p_2)\cdot p_3 - p_{3\mu}(p_1+p_2)_\nu\right]\\
&\quad\epsilon^\nu(p_3)\,D(p_1,p_2,p_3)\,.
\end{aligned}
\tag{35}
$$

We again present the results in the form

$$
D^{(\alpha)}(p_1,p_2,p_3) = \sum_{j=1}^{5} P_j^{(\alpha)} T_j \qquad \alpha = 1,2,3
\tag{36}
$$

with the basis of the scalar integrals:

$$
\begin{aligned}
&T_1 = 1\\
&T_2 = 2[1-g(\tau_s)] && T_3 = 2[1-g(\tau_H)]\\
&T_4 = 2f(\tau_s) && T_5 = 2f(\tau_H)\,.
\end{aligned}
\tag{37}
$$

The coefficients corresponding to the SM and the Yukawa modifying operator in the SMEFT case read:

$$
\begin{aligned}
P_1^{(1)} &= \frac{8}{(\tilde{s}-\rho)}\\
P_2^{(1)} &= \frac{8\tilde{s}}{(\tilde{s}-\rho)^2}\\
P_3^{(1)} &= -\frac{8\tilde{s}}{(\tilde{s}-\rho)^2}\\
P_4^{(1)} &= -\frac{4\,(4+\tilde{s}-\rho)}{(\tilde{s}-\rho)^2}\\
P_5^{(1)} &= \frac{4\,(4+\tilde{s}-\rho)}{(\tilde{s}-\rho)^2}\,.
\end{aligned}
\tag{38}
$$

The contribution of the chromomagnetic operator reads:

$$
\begin{aligned}
P_1^{(3)} &= \frac{4\left[\rho+2(\tilde{s}-\rho)\ln\frac{\mu_R^2}{m_t^2}\right]}{(\tilde{s}-\rho)}\\
P_2^{(3)} &= \frac{2\left[2\tilde{s}^2+(\tilde{s}-\rho)^2\right]}{(\tilde{s}-\rho)^2}
\end{aligned}
$$

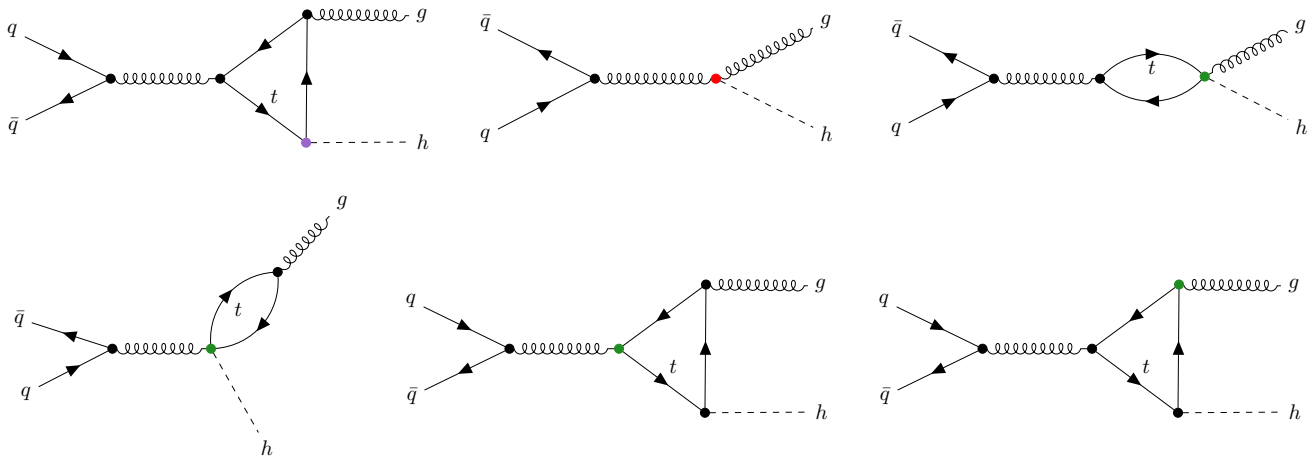

Fig. 4 Generic diagrams of the $q\bar{q}$-channel diagrams in the SMEFT. The color coding is the same as in Figs. 1–3

$$P_3^{(3)} = -\frac{4\rho\,(2\tilde{s}-\rho)}{(\tilde{s}-\rho)^2}$$
$$P_4^{(3)} = -\frac{8(2\tilde{s}-\rho)}{(\tilde{s}-\rho)^2}$$
$$P_5^{(3)} = \frac{8(2\tilde{s}-\rho)}{(\tilde{s}-\rho)^2}. \tag{39}$$

Again, we finalise the results by presenting the amplitude for the point-like Higgs coupling to gluons which corresponds to the HTL of the SM:

$$D^{(2)}(p_1, p_2, p_3) = -16\,. \tag{40}$$

The HTL of the relevant operators reads:

$$D^{(1)} \to \frac{1}{12}D^{(2)} = -\frac{4}{3}$$
$$D^{(3)} \to \frac{1}{2}(1 - \ln\frac{\mu_R^2}{m_t^2})D^{(2)} = -8\left(1 - \ln\frac{\mu_R^2}{m_t^2}\right).$$

The final expression for the form factor is given by

$$\begin{aligned} &D(p_1, p_2, p_3) \\ &\quad = c_1 D^{(1)}(p_1, p_2, p_3) + c_2(\mu_R) D^{(2)}(p_1, p_2, p_3) \\ &\qquad + Re(c_3)\frac{m_t^2}{v^2} D^{(3)}(p_1, p_2, p_3)\,. \end{aligned} \tag{41}$$

The result for the qg channel can be obtained by crossing.

The above results allow us to obtain complete predictions for Higgs boson production at high p_T in the SMEFT. In Ref. [42] the effects of the $\mathcal{O}_1$ and $\mathcal{O}_2$ were studied, including the resummation of the large logarithmic contributions at small p_T, but neglecting the contribution of the chromomagnetic operator. We thus focus here on the effect of the chromomagnetic operator at high p_T. We consider pp collisions at $\sqrt{s} = 13$ TeV and use PDF4LHC2015 NLO parton distributions [50–55]. The central value of the renormalization and factorization scales is fixed to $\mu_F = \mu_R = 0.5 \times \sqrt{m_H^2 + p_T^2}$.

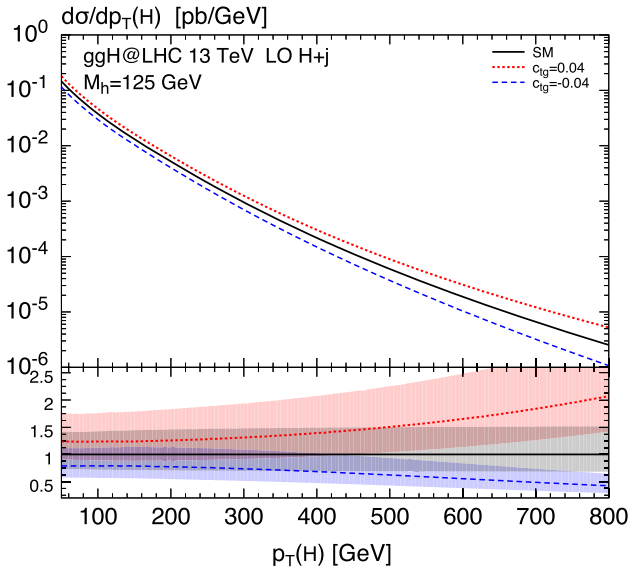

Fig. 5 Impact of the chromomagnetic operator on the p_T spectrum of the Higgs boson in the region allowed by the current experimental constraints

In Fig. 5 we show the impact of the operator $\mathcal{O}_3$, by considering a variation of the coefficient c_3 within the range suggested by the study of Ref. [56]. The p_T spectrum including the impact of the chromomagnetic operator is normalised to the SM result. Perturbative uncertainties are estimated with the usual 7-point scale variations. The numerical results, obtained with a modified version of the program HIGLU [57], show that the chromomagnetic operator can significantly affect the p_T spectrum, and the effects start to exceed the scale uncertainty of the SM result around $p_T \approx 400$–500 GeV. Considering also the improvements in the theoreti-

cal control of the SM prediction [21–23,28], this means that at large transverse momenta the effect of the chromomagnetic operator could be clearly discriminated with respect to the SM prediction. Our numerical results agree with those of Ref. [40]. A more detailed study will be presented elsewhere.

4 Conclusions

In this work we studied Higgs boson production at large transverse momentum in gluon fusion within the SMEFT. We provided explicit and compact analytical results for the one-loop matrix elements of the corresponding partonic processes $gg, q\bar{q} \to Hg$ and $gq \to Hq$. The results, which are expressed in terms of standard one-loop scalar integrals, require the renormalization of the dimension-six point-like Higgs coupling to gluons in accordance with the related renormalization of the inclusive cross section [38,42]. We studied the quantitative impact of the chromomagnetic operator and found that it can significantly distort the transverse-momentum spectrum of the Higgs boson at large p_T. Depending on the actual size of the corresponding Wilson coefficient, this contribution has to be taken into account for a solid study of relevant dimension-six operators within the SMEFT. Turning this argument around, the Higgs transverse-momentum distribution will provide a relevant observable to constrain the Wilson coefficient of the chromomagnetic operator when significant statistics is accumulated.

Acknowledgements We would like to thank Fabio Maltoni and Eleni Vryonidou for useful correspondence on the results of Ref. [40]. This research was supported in part by the Swiss National Science Foundation (SNF) under contracts CRSII2-141847, 200020-169041 and by the Research Executive Agency (REA) of the European Union under the Grant Agreement number PITN–GA–2012–316704 (*HiggsTools*).

Funded by SCOAP[3].

Appendix: Scalar integrals

In this appendix we present the definitions of the functions f, g, J used for our analytical results and their relation to the scalar one-loop integrals.

$$g(\tau) = \begin{cases} \sqrt{\tau-1}\arcsin\dfrac{1}{\sqrt{\tau}} & \tau \geq 1 \\ \dfrac{\sqrt{1-\tau}}{2}\left[\ln\dfrac{1+\sqrt{1-\tau}}{1-\sqrt{1-\tau}} - i\pi\right] & \tau < 1 \end{cases}. \quad (42)$$

$$f(\tau) = \begin{cases} \arcsin^2\dfrac{1}{\sqrt{\tau}} & \tau \geq 1 \\ -\dfrac{1}{4}\left[\ln\dfrac{1+\sqrt{1-\tau}}{1-\sqrt{1-\tau}} - i\pi\right]^2 & \tau < 1 \end{cases} \quad (43)$$

$$\begin{aligned} J(\tilde{s},\tilde{t},\tilde{u}) &= I_3(\tilde{s},\tilde{t},\tilde{u},\tilde{s}) + I_3(\tilde{s},\tilde{t},\tilde{u},\tilde{u}) - I_3(\tilde{s},\tilde{t},\tilde{u},\rho) \\ I_3(\tilde{s},\tilde{t},\tilde{u},\tilde{x}) &= \frac{1}{\tilde{s}\tilde{u}}\frac{2}{\beta_+-\beta_-}\left(\mathrm{Li}_2\left(\frac{\beta_-}{\beta_--\alpha_-}\right)\right. \\ &\quad -\mathrm{Li}_2\left(\frac{\beta_+}{\beta_+-\alpha_+}\right) + \mathrm{Li}_2\left(\frac{\beta_-}{\beta_--\alpha_+}\right) \\ &\quad \left.-\mathrm{Li}_2\left(\frac{\beta_+}{\beta_+-\alpha_-}\right) + \log\left(-\frac{\beta_+}{\beta_-}\right)\log\left(1+\frac{\tilde{x}\tilde{t}}{\tilde{s}\tilde{u}}\right)\right), \end{aligned} \quad (44)$$

with $\alpha_\pm = \frac{1}{2}(1 \pm \sqrt{1-\frac{4}{\tilde{x}}})$ and $\beta_\pm = \frac{1}{2}(1 \pm \sqrt{1-\frac{4\tilde{t}}{\tilde{s}\tilde{u}}})$. The function Li_2 denotes the Spence function. The functions f, g, J are related to the corresponding scalar one-loop integrals as ($n = 4 - 2\epsilon$)

$$\begin{aligned} &B_0(p; m_t, m_t) = \int \frac{d^nk}{(2\pi)^n}\frac{\mu^{2\epsilon}}{(k^2-m_t^2)[(k+p)^2-m_t^2]} \\ &= i\frac{\Gamma(1+\epsilon)}{(4\pi)^2}\left(\frac{4\pi\mu^2}{m_t^2}\right)^\epsilon\left[\frac{1}{\epsilon}+2-2g(\tau)\right]+\mathcal{O}(\epsilon) \\ &\quad (\tau = 4m_t^2/p^2) \\ &C_0(p_1,p_2;m_t,m_t,m_t) \\ &= \int \frac{d^nk}{(2\pi)^n}\frac{\mu^{2\epsilon}}{(k^2-m_t^2)[(k-p_1)^2-m_t^2][(k+p_2)^2-m_t^2]} \\ &= \frac{i}{(4\pi)^2 m_t^2}\left[-\frac{\tau}{2}f(\tau)\right]+\mathcal{O}(\epsilon) \qquad (\tau = 4m_t^2/(2p_1p_2)) \\ &D_0(p_1,p_2,p_3;m_t,m_t,m_t,m_t) \\ &= \int \frac{d^nk}{(2\pi)^n} \\ &\quad \times \frac{\mu^{2\epsilon}}{(k^2-m_t^2)[(k+p_1)^2-m_t^2][(k+p_{12})^2-m_t^2][(k+p_{123})^2-m_t^2]} \\ &= \frac{i}{(4\pi)^2 m_t^4}J\left(\frac{s}{m_t^2},\frac{t}{m_t^2},\frac{u}{m_t^2}\right)+\mathcal{O}(\epsilon) \end{aligned} \quad (45)$$

where $p_{12} = p_1 + p_2, p_{123} = p_1 + p_2 + p_3$ and $s = 2p_1p_2, t = 2p_1p_3, u = 2p_2p_3$ where all p_i ($i = 1, 2, 3$) correspond to incoming massless external particles ($p_i^2 = 0$).

References

1. ATLAS Collaboration, G. Aad et al., Observation of a new particle in the search for the Standard Model Higgs boson with the ATLAS detector at the LHC, Phys. Lett. B **716**, 1–29 (2013). arXiv:1207.7214
2. CMS Collaboration, S. Chatrchyan et al., Observation of a new boson at a mass of 125 GeV with the CMS experiment at the LHC. Phys. Lett. B **716**, 30–61 (2013). arXiv:1207.7235
3. ATLAS, CMS Collaboration, G. Aad et al., Measurements of the Higgs boson production and decay rates and constraints on its couplings from a combined ATLAS and CMS analysis of the LHC

pp collision data at $\sqrt{s} = 7$ and 8 TeV, JHEP **08**, 045 (2016). arXiv:1606.02266
4. LHC Higgs Cross Section Working Group Collaboration, J. R. Andersen et al., Handbook of LHC Higgs Cross Sections: 3. Higgs Properties. arXiv:1307.1347
5. LHC Higgs Cross Section Working Group Collaboration, D. de Florian et al., Handbook of LHC Higgs Cross Sections: 4. Deciphering the Nature of the Higgs Sector. arXiv:1610.07922
6. HiggsTools Working Group Collaboration, M. Boggia et al., The HiggsTools Handbook: Concepts and observables for deciphering the Nature of the Higgs Sector. arXiv:1711.09875
7. W. Buchmuller, D. Wyler, Effective Lagrangian analysis of new interactions and flavor conservation. Nucl. Phys. B **268**, 621–653 (1986)
8. B. Grzadkowski, M. Iskrzynski, M. Misiak, J. Rosiek, Dimension-six terms in the Standard Model Lagrangian. JHEP **10**, 085 (2010). arXiv:1008.4884
9. ATLAS Collaboration, G. Aad et al., Measurements of fiducial and differential cross sections for Higgs boson production in the diphoton decay channel at $\sqrt{s} = 8$ TeV with ATLAS, JHEP **09**, 112 (2014). arXiv:1407.4222
10. ATLAS Collaboration, G. Aad et al., Fiducial and differential cross sections of Higgs boson production measured in the four-lepton decay channel in pp collisions at $\sqrt{s}$=8 TeV with the ATLAS detector, Phys. Lett. B **738**, 234–253 (2014). arXiv:1408.3226
11. ATLAS Collaboration, G. Aad et al., Measurements of the Total and Differential Higgs Boson Production Cross Sections Combining the $H \to \gamma\gamma$ and $H \to ZZ^* \to 4l$ Decay Channels at $\sqrt{s}$=8??TeV with the ATLAS Detector, Phys. Rev. Lett. **115**(9), 091801 (2015). arXiv:1504.05833
12. ATLAS Collaboration, G. Aad et al., Measurement of fiducial differential cross sections of gluon-fusion production of Higgs bosons decaying to WW$^* \to e\nu\mu\nu$ with the ATLAS detector at $\sqrt{s} = 8$ TeV, JHEP **08**, 104 (2016). arXiv:1604.02997
13. CMS Collaboration, S. Chatrchyan et al., Measurement of differential cross sections for Higgs boson production in the diphoton decay channel in pp collisions at $\sqrt(s) = 8$ TeV. arXiv:1508.07819 (2015). arXiv:1508.07819
14. CMS Collaboration, V. Khachatryan et al., Measurement of differential and integrated fiducial cross sections for Higgs boson production in the four-lepton decay channel in pp collisions at $\sqrt{s} = 7$ and 8 TeV. JHEP **04**, 005 (2016). arXiv:1512.08377
15. CMS Collaboration, V. Khachatryan et al., Measurement of the transverse momentum spectrum of the Higgs boson produced in pp collisions at $\sqrt{s} = 8$ TeV using $H \to WW$ decays. JHEP **03**, 032 (2017). arXiv:1606.01522
16. ATLAS Collaboration, M. Aaboud et al., Measurement of inclusive and differential cross sections in the $H \to ZZ^* \to 4\ell$ decay channel in pp collisions at $\sqrt{s} = 13$ TeV with the ATLAS detector, JHEP **10**, 132 (2017). arXiv:1708.02810
17. ATLAS Collaboration, M. Aaboud et al., Measurements of Higgs boson properties in the diphoton decay channel with 36 fb^{-1} of pp collision data at $\sqrt{s} = 13$ TeV with the ATLAS detector. arXiv:1802.04146
18. CMS Collaboration, A.M. Sirunyan et al., Measurements of properties of the Higgs boson decaying into the four-lepton final state in pp collisions at $\sqrt{s} = 13$ TeV. JHEP **11**, 047 (2017). arXiv:1706.09936
19. A. Banfi, A. Martin, V. Sanz, Probing top-partners in Higgs+jets. JHEP **08**, 053 (2014). arXiv:1308.4771
20. A. Azatov, C. Grojean, A. Paul, E. Salvioni, Resolving gluon fusion loops at current and future hadron colliders. JHEP **09**, 123 (2016). arXiv:1608.00977
21. R. Boughezal, F. Caola, K. Melnikov, F. Petriello, M. Schulze, Higgs boson production in association with a jet at next-to-next-to-leading order in perturbative QCD. JHEP **06**, 072 (2013). arXiv:1302.6216
22. R. Boughezal, F. Caola, K. Melnikov, F. Petriello, M. Schulze, Higgs boson production in association with a jet at next-to-next-to-leading order. Phys. Rev. Lett. **115**(8), 082003 (2015). arXiv:1504.07922
23. X. Chen, T. Gehrmann, E.W.N. Glover, M. Jaquier, Precise QCD predictions for the production of Higgs + jet final states. Phys. Lett. B **740**, 147–150 (2015). arXiv:1408.5325
24. R. Bonciani, V. Del Duca, H. Frellesvig, J.M. Henn, F. Moriello, V.A. Smirnov, Two-loop planar master integrals for Higgs→ 3 partons with full heavy-quark mass dependence. JHEP **12**, 096 (2016). arXiv:1609.06685
25. K. Kudashkin, K. Melnikov, C. Wever, Two-loop amplitudes for processes $gg \to Hg, qg \to Hq$ and $q\bar{q} \to Hg$ at large Higgs transverse momentum. JHEP **02**, 135 (2018). arXiv:1712.06549
26. J .M. Lindert, K. Kudashkin, K. Melnikov, C. Wever, Higgs bosons with large transverse momentum at the LHC. Phys. Lett. **B782**, 210–214 (2018). arXiv:1801.08226
27. T. Neumann, NLO Higgs+jet at Large transverse momenta including top quark mass effects. arXiv:1802.02981
28. S.P. Jones, M. Kerner, G. Luisoni, Next-to-leading-order QCD corrections to Higgs Boson Plus jet production with full Top-quark mass dependence. Phys. Rev. Lett. **120**(16), 162001 (2018). arXiv:1802.00349
29. G. Brooijmans et al., Les Houches 2015: Physics at TeV colliders—new physics working group report. arXiv:1605.02684
30. R.V. Harlander, S. Liebler, H. Mantler, SusHi Bento: beyond NNLO and the heavy-top limit. Comput. Phys. Commun. **212**, 239–257 (2017). arXiv:1605.03190
31. C. Anastasiou, C. Duhr, F. Dulat, E. Furlan, T. Gehrmann, F. Herzog, A. Lazopoulos, B. Mistlberger, CP-even scalar boson production via gluon fusion at the LHC. JHEP **09**, 037 (2016). arXiv:1605.05761
32. C. Grojean, E. Salvioni, M. Schlaffer, A. Weiler, Very boosted Higgs in gluon fusion. JHEP **05**, 022 (2014). arXiv:1312.3317
33. A. Azatov, A. Paul, Probing Higgs couplings with high p_T Higgs production. JHEP **01**, 014 (2014). arXiv:1309.5273
34. U. Langenegger, M. Spira, I. Strebel, Testing the Higgs Boson coupling to gluons (2015). arXiv:1507.01373. arXiv:1507.01373
35. R.V. Harlander, T. Neumann, Probing the nature of the Higgs-gluon coupling. Phys. Rev. D **88**, 074015 (2013). arXiv:1308.2225
36. S. Dawson, I.M. Lewis, M. Zeng, Effective field theory for Higgs boson plus jet production. Phys. Rev. D **90**(9), 093007 (2014). arXiv:1409.6299
37. D. Choudhury, P. Saha, Higgs production as a probe of anomalous top couplings. JHEP **08**, 144 (2012). arXiv:1201.4130
38. C. Degrande, J.M. Gerard, C. Grojean, F. Maltoni, G. Servant, Probing Top-Higgs non-standard interactions at the LHC. JHEP **07**, 036 (2012). arXiv:1205.1065 [Erratum: JHEP03,032(2013)]
39. C. Zhang, Automating predictions for standard model effective field theory in MadGraph5 aMC@NLO, PoS**RADCOR2015**, 101 (2016). arXiv:1601.03994
40. F. Maltoni, E. Vryonidou, C. Zhang, Higgs production in association with a top-antitop pair in the Standard Model Effective Field Theory at NLO in QCD. JHEP **10**, 123 (2016). arXiv:1607.05330
41. N. Deutschmann, C. Duhr, F. Maltoni, E. Vryonidou, Gluon-fusion Higgs production in the Standard Model Effective Field Theory. JHEP **12**, 063 (2017). arXiv:1708.00460
42. M. Grazzini, A. Ilnicka, M. Spira, M. Wiesemann, Modeling BSM effects on the Higgs transverse-momentum spectrum in an EFT approach. JHEP **03**, 115 (2017). arXiv:1612.00283
43. G.F. Giudice, C. Grojean, A. Pomarol, R. Rattazzi, The strongly-interacting light Higgs. JHEP **06**, 045 (2007). arXiv:hep-ph/0703164

44. R. Contino, M. Ghezzi, C. Grojean, M. Muhlleitner, M. Spira, Effective Lagrangian for a light Higgs-like scalar. JHEP **07**, 035 (2013). arXiv:1303.3876
45. M. Grazzini, A. Ilnicka, M. Spira, M. Wiesemann, Effective Field Theory for Higgs properties parametrisation: the transverse momentum spectrum case, 52nd Rencontres de Moriond QCD 2017, La Thuile (2017). arXiv:1705.05143
46. M. Grazzini, A. Ilnicka, M. Spira, M. Wiesemann, Effective field theory in quest to parametrise Higgs properties: the transverse momentum spectrum case. J. Phys. Conf. Ser. **873**(1), 012050 (2017)
47. M. Spira, Radiative QCD corrections to decay and production of Higgs bosons at e+e- and pp accelerators (in German), PhD thesis, Aachen, Tech. Hochsch. (1993)
48. M. Spira, A. Djouadi, D. Graudenz, P.M. Zerwas, Higgs boson production at the LHC. Nucl. Phys. B **453**, 17–82 (1995). arXiv:hep-ph/9504378
49. R.K. Ellis, I. Hinchliffe, M. Soldate, J.J. van der Bij, Higgs decay to tau+ tau-: a possible signature of intermediate Mass Higgs Bosons at the SSC. Nucl. Phys. B **297**, 221 (1988)
50. J. Butterworth et al., PDF4LHC recommendations for LHC Run II. J. Phys. **G 43**, 023001 (2016). arXiv:1510.03865
51. **NNPDF** Collaboration, R. D. Ball et al., Parton distributions for the LHC Run II, JHEP **04**, 040 (2015). arXiv:1410.8849
52. S. Dulat, T.-J. Hou, J. Gao, M. Guzzi, J. Huston, P. Nadolsky, J. Pumplin, C. Schmidt, D. Stump, C.P. Yuan, New parton distribution functions from a global analysis of quantum chromodynamics. Phys. Rev. D **93**(3), 033006 (2016). arXiv:1506.07443
53. L.A. Harland-Lang, A.D. Martin, P. Motylinski, R.S. Thorne, Parton distributions in the LHC era: MMHT 2014 PDFs. Eur. Phys. J. C **75**(5), 204 (2015). arXiv:1412.3989
54. J. Gao, P. Nadolsky, A meta-analysis of parton distribution functions. JHEP **07**, 035 (2014). arXiv:1401.0013
55. S. Carrazza, S. Forte, Z. Kassabov, J.I. Latorre, J. Rojo, An unbiased Hessian representation for Monte Carlo PDFs. Eur. Phys. J. C **75**(8), 369 (2015). arXiv:1505.06736
56. D. Buarque Franzosi, C. Zhang, Probing the top-quark chromomagnetic dipole moment at next-to-leading order in QCD. Phys. Rev. D **91**(11), 114010 (2015). arXiv:1503.08841
57. M. Spira, HIGLU: a program for the calculation of the total Higgs production cross-section at hadron colliders via gluon fusion including QCD corrections. arXiv:hep-ph/9510347 (1995)